

S-Rich PbS Quantum Dots: A Promising p-Type Material for Optoelectronic Devices

Journal Article

Author(s):

Bederak, Dmytro; [Dirin, Dmitry](#) ; Sukharevska, Nataliia; Momand, Jamo; Kovalenko, Maksym V.; Loi, Maria A.

Publication date:

2021-01-12

Permanent link:

<https://doi.org/https://doi.org/10.3929/ethz-b-000468151>

Rights / license:

[Creative Commons Attribution-NonCommercial-NoDerivatives 4.0 International](#)

Originally published in:

Chemistry of Materials 33(1), <https://doi.org/10.1021/acs.chemmater.0c03865>

S-Rich PbS Quantum Dots: A Promising p-Type Material for Optoelectronic Devices

Dmytro Bederak,¹ Dmitry N. Dirin,¹ Nataliia Sukharevska, Jamo Momand, Maksym V. Kovalenko,* and Maria A. Loi*



Cite This: *Chem. Mater.* 2021, 33, 320–326



Read Online

ACCESS |



Metrics & More

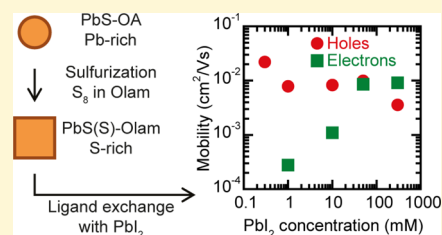


Article Recommendations



Supporting Information

ABSTRACT: PbS colloidal quantum dots (CQDs) are versatile building blocks for bottom-up fabrication of various optoelectronic devices. The transport properties of thin films of this class of materials depend on the size of the CQDs, their surface ligands, and stoichiometry. The most common synthetic methods yield PbS CQDs with an excess of Pb atoms, which induces n-type transport properties in CQD films. In this work, we developed a new synthesis, which offers S-rich PbS CQDs. Thanks to their sufficient colloidal stability in nonpolar solvents, we established a protocol for the integration of these CQDs into thin field-effect transistors and found strong hole-dominated transport with a hole mobility of about $1 \times 10^{-2} \text{ cm}^2/\text{Vs}$. Moreover, we were able to enhance the electron mobility for almost two orders of magnitude while keeping the hole mobility nearly the same. This approach allows us to obtain reliably p-doped PbS CQDs, which can be used for the fabrication of various electronic and optoelectronic devices.



INTRODUCTION

Colloidal inorganic semiconductor nanocrystals (colloidal quantum dots, CQDs) are among the most versatile nanoscale materials owing to their tunable optoelectronic properties, easily adaptable surface chemistry, and simplicity of their deposition with solution-based techniques. The performance of CQD-based photovoltaic and light-emitting devices has been persistently improving in the last years, and it competes now closely with the one of the other solution-processable materials.¹ Lead chalcogenide CQDs are the most commonly used type of CQDs for photovoltaic devices due to their tunable band gap (from visible to near-infrared), high dielectric constant, strong light absorption, high perfectness of the synthetically accessible quality, good stability, and the claimed possibility to overcome the Shockley–Queisser limit by using multiple exciton generation.² At the moment, the most efficient lead chalcogenide CQD solar cells are based on PbS, and their record power conversion efficiency reached 13.8%.³

There are three common synthetic approaches to high-quality colloidal PbS CQDs in the literature.^{4–6} Despite the large difference in the initial steps of synthetic protocols and some dissimilarities in the surface chemistry, all three approaches give rise to PbS CQDs capped with lead oleate. Lead oleate ligands provide Pb-rich composition to the otherwise stoichiometric PbS core.⁷ It is well-known that the stoichiometry of PbS CQDs has a crucial effect on the electronic structure of CQD solids. Thus, an excess of lead atoms on the surface of the CQDs results in electron favorable transport properties (n-type transport).⁸ In contrast, how to

achieve a high, reliable, and tunable level of p-doping is a long-lived research question, as an insufficient p-doping of the p-type layer composing PbS CQD solar cells was identified as one of their performance-limiting factors.⁹

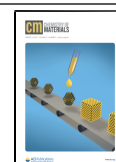
Nowadays, the hole transporting layer of the most efficient PbS CQD solar cells utilizes CQDs treated with 1,2-ethanedithiol or 3-mercaptopropionic acid, which can donate extra states to the valence band of CQDs. Still, such films exhibit ambipolar transport properties with electron-dominated transport when processed air-free.^{10,11} An efficient p-type transport in these solids is only achieved upon their exposure to air.^{12–15} However, the p-doping by oxygen shows a strong dependence on the humidity of the environment, which can cause high irreproducibility between the devices fabricated at different places or at different times during the year.¹⁶ In addition to the difficulties in controlling the oxygen doping of the CQD films, air exposure of the CQD film could result in adsorption of water or undesirable atmospheric contaminants and impact on trap densities and charge carrier mobilities.¹⁷

A few methods were demonstrated to shift the stoichiometry of PbS CQDs and to form S-rich p-type CQD solids. These methods include thermal evaporation of elemental sulfur onto

Received: September 30, 2020

Revised: November 27, 2020

Published: December 10, 2020



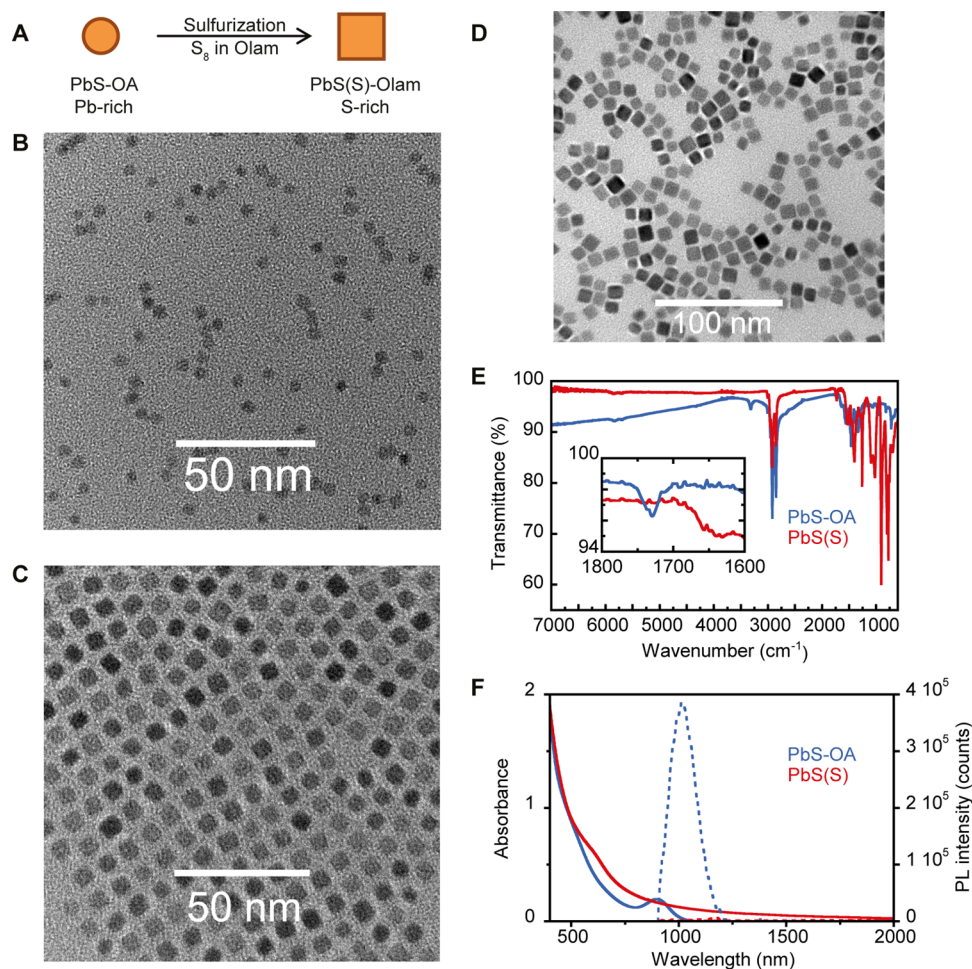


Figure 1. (A) Schematic illustration of the sulfurization process of oleate-capped PbS (PbS-OA) CQDs. (B) TEM image of PbS-OA CQDs. (C) TEM image of PbS CQDs after the sulfurization (PbS(S)). (D) TEM image of PbS(S) CQDs after the sulfurization for longer time using three times higher amount of sulfurization reagent. (E) FTIR spectra of oleate-capped PbS-OA and PbS(S) CQDs. The inset shows the zoomed double bond region. (F) Absorption (solid lines) and photoluminescence spectra (dashed lines) of PbS-OA and PbS(S) CQDs.

CQD solids^{18,19} and treatment of CQDs with an organosulfur compound,²⁰ mostly using two-step solution-processable ligand exchange.^{17,21} However, all these approaches are based on the postdeposition film sulfurization, which complicates the device fabrication and provides limited compatibility with large-scale device fabrication.

Here, we propose a new synthetic strategy for S-rich PbS CQDs by sulfurization of oleate-capped Pb-rich CQDs in solution. We developed a ligand exchange protocol for these CQDs and characterized the electrical transport properties of the resultant films in field-effect transistors. Our ligand exchange method can be used for the fine-tuning of the transport properties by affecting mainly the electron transport, while keeping the hole transport almost unchanged. These novel S-rich PbS CQDs do not require air exposure for efficient hole transport, thus eliminating the need for poorly controllable fabrication steps.

EXPERIMENTAL SECTION

Materials. Lead (II) acetate trihydrate ($\text{Pb}(\text{CH}_3\text{COO})_2 \times 3\text{H}_2\text{O}$, $\geq 99.99\%$, Aldrich), bis(trimethylsilyl)sulfide (TMS_2S , Aldrich), 1-octadecene (ODE, 90%, Aldrich), oleic acid (OA, 90%, Aldrich), sulfur powder (S, 99.998%, Aldrich), oleylamine (Olam, 95%, STREM), ethanol (Fluka), hexane (Aldrich), ethyl acetate (extra dry, 99.9%, Acros), lead (II) iodide (PbI_2 , 99.99%, TCI), and *N,N*-

dimethylformamide (DMF, extra dry, 99.8%, Acros) were used as received.

Oleate-Capped PbS CQD Synthesis. PbS-OA CQDs were synthesized according to the method of Hines et al.⁴ with slight modifications as described elsewhere.²² For obtaining 3.0 nm PbS-OA CQDs, $\text{Pb}(\text{CH}_3\text{COO})_2 \times 3\text{H}_2\text{O}$ (1.5 g, 4 mmol), ODE (47.5 mL), and oleic acid (2.5 mL, 7.07 mmol) were mixed in a three-neck flask. The mixture was degassed under vacuum at 120 °C for 1 h and refilled with nitrogen. The temperature was set to 90 °C. After reaching this temperature, the heating mantle was removed and solution of TMS_2S (0.42 mL, 2 mmol) in 10 mL of ODE (dried) was injected into vigorously stirring lead oleate solution at 85 °C. After 1 min of CQD growth, the reaction was quenched by injecting 3 mL of dried OA and cooling down the mixture with an ice bath. CQDs were washed three times with the hexane/ethanol solvent/nonsolvent pair (30/144, 30/36, and 15/17 mL at first, second, and third washing cycles, respectively), redissolved in anhydrous hexane under an N_2 atmosphere, and filtered through 0.2 μm PTFE filter.

Sulfurization of PbS-OA CQDs. PbS(S)-Olam CQDs were synthesized by treating PbS-OA CQDs with sulfur solution in Olam in a nitrogen atmosphere. This solution has been prepared by dissolving 480 mg of sulfur in 15 mL of dried Olam over 3 h at 60 °C inside a glovebox. PbS-OA (450 mg) in 3.3 mL of hexane was added to this S-Olam solution, and the mixture was stirred for 3 h at 60 °C. The obtained PbS(S)-Olam CQDs were precipitated using 120 mL of ethyl acetate and redissolved in 10 mL of anhydrous hexane.

PbS CQD Thin-Film Field-Effect Transistor (FET) Fabrication and Measurements. The PbS CQD FETs were fabricated on top of highly doped Si substrates covered with a 230 nm thermally grown SiO₂ dielectric. A prepatterned interdigitated source and drain ITO/Au (10 nm/30 nm) electrodes formed a channel with 1 cm in width and 20 μm in length. The substrates were cleaned by sequential sonication in acetone and isopropanol and dried in the oven. The CQD film was deposited from 20 mg/mL dispersion of S-rich CQDs capped with native ligands by spin-coating from hexane dispersion at 1000 rpm. The solid-state ligand exchange was performed by soaking a film into a PbI₂ solution in DMF for 1 min and washing with DMF. The device fabrication was finished by drying the film at 120 °C for 1 min (so-called “fresh” devices). The devices referred in the text as “annealed” were annealed on a hotplate for 20 min at 120 °C after the fabrication. All transistor measurements were performed with an Agilent E5262A semiconductor parameter analyzer. All fabrication and measurement steps were performed in N₂-filled gloveboxes with O₂ and H₂O levels below 0.1 ppm. The hole and electron mobility values were extracted from the transfer (I_D–V_G) characteristics of the FETs in the linear regime using the gradual channel approximation and the parallel plate capacitance of the oxide layer.

Absorbance and PL Measurements. UV/vis/IR absorption spectra were collected using a Jasco V670 or Shimadzu UV-3600 spectrometer. PL spectra were recorded using a Jasco V670 spectrometer.

FTIR Spectroscopy. Attenuated total reflectance FTIR spectra of PbS and PbS(S) CQDs were recorded using a Thermo Scientific Nicolet iS5 FTIR spectrometer. The samples after the ligand exchange with PbI₂ were deposited on double-polished silicon substrates following the FET fabrication protocol. FTIR spectra were obtained by using a Shimadzu IRTracer-100 spectrometer.

Rutherford Backscattering Spectrometry (RBS). The samples for RBS were prepared on silicon wafers using the method described earlier. The composition was determined by 2-MeV He RBS at the ETH Laboratory of Ion Beam Physics using a silicon PIN diode detector under 168°. The relatively high energy of the beam used for the analysis allowed the separation of all the peaks of the relevant elements. The data were analyzed with the RUMP software to obtain the stoichiometry.²³

Electron Microscopy. TEM, electron diffraction, and EDX data were collected using a JEOL JEM-2010 microscope operated at 200 keV. Samples were prepared by drop-casting a diluted PbS CQD dispersion in hexane onto carbon-coated Cu grids. The ligand exchange with S-rich CQDs was done by immersing the grid into 300 mM PbI₂ solution in DMF for 1 min followed by washing in pure DMF. EDX spectra were measured by using a SiLi detector cooled down with liquid nitrogen. All the samples were measured in the same conditions such as the size of condenser aperture, magnification, spot and beam sizes, tilt of the holder, and the detector measurement rate. From 10 to 15 different spots located in different openings of the grid were analyzed for every sample. The spectra were fitted with the Cliff-Lorimer (MTBS) method without absorbance by using the NSS software version 3.1 from Thermo Scientific. Deconvolution of Pb Mα and S Kα peaks was done automatically by the software. The size distribution of S-rich PbS(S) CQDs was obtained from the TEM micrograph by using ImageJ software assuming an ideal cubic shape of the nanoparticles.

RESULTS AND DISCUSSION

For the formation of the S-rich PbS(S) CQDs, sulfurization of the PbS CQDs was performed by using elemental sulfur dissolved in oleylamine (S-Olam). This process is schematically illustrated in Figure 1A. Sulfur dissolved in Olam is known to produce a range of ammonium and alkylammonium sulfides and polysulfides.^{24–27} Annealing of lead oleate-capped PbS CQDs in such conditions should lead to the reaction of surface lead oleate with sulfide groups and therefore growth of an extra monolayer of PbS and exchange from oleate to

alkylammonium sulfide ligands. Furthermore, a strong excess of alkylammonium sulfides and the elevated temperature of the whole process are expected to initiate the ripening of CQDs.

Upon sulfurization, the spherical oleate-capped PbS CQDs (Figure 1B) grow in size and change their shape into cubic. These transformations are revealed from the TEM micrographs (Figure 1B–D). The extent of these transformations depends on the initial size of PbS CQDs, the ratio between the CQDs and the S-Olam, and the reaction time. For example, 5.4 nm PbS CQDs treated with S-Olam for 1 hour almost do not grow although they still change shape to cubic (Figure 1C). In contrast, 2.9 nm PbS CQDs treated with three times larger amounts of S-Olam for 3 h in otherwise the same conditions increase their average size to 8.6 nm (Figure 1D). Such size-dependent ripening may be related to either or a combination of the two following possible reasons:

- faster growth of CQDs along the polar (111) axis; smaller PbS CQDs are known to have a higher fraction of polar Pb-terminated (111) facets compared to the larger CQDs, which have a more stoichiometric surface.^{28,29}
- faster ripening of CQDs in higher excess of precursors. Smaller PbS CQDs have a higher excess of lead. For small (~3 nm) CQDs, the Pb/S ratio can be well above 1.5, whereas for large (>7 nm) CQDs, the Pb/S ratio is reduced to 1.1–1.26.^{28,29} Since our method for recapping CQDs with sulfur implies a substantial excess of sulfur precursor, this creates a higher concentration of both PbS precursors for small CQDs compared to the large ones. Larger amounts of both precursors should lead to faster ripening of CQDs.

The size distribution of the obtained S-rich PbS(S) CQDs is shown in Figure S1. The lattice constant extracted from the high-resolution TEM image of a single S-rich PbS(S) CQD is 0.5926 nm (Figure S2), which corresponds to the lattice constant of the PbS rock salt crystal structure (0.594 nm). The selected area electron diffraction (SAED) pattern of S-rich PbS(S) CQDs with native ligands is shown in Figure S3. The majority of the nanocubes, as expected, are oriented along the <100> axis, giving rise to intense reflections from the (200), (220), (400), and (420) planes. From the electron diffraction experiment, the fitted lattice constant was found to be 0.5942 nm, which confirms that nanocubes are composed of PbS in the typical rock salt crystal structure.

As mentioned above, sulfurization of PbS CQDs replaces oleate ligands for alkylammonium sulfides, as evidenced by the disappearance of carboxylic C=O group vibration at 1730 cm⁻¹ in the FTIR spectra (Figure 1E). Alkylammonium salts often form micelles in nonpolar solvents and weakly bound to the surface of CQDs. These factors significantly increase the amount of organics in colloidal solution and complicate washing of alkylammonium-passivated CQDs – a well-known problem among researchers working with colloidal lead halide perovskite nanocrystals.^{5,30} Indeed, dried pellets of PbS(S) CQDs washed with conventional antisolvents, e.g., ethanol or acetone, contained more than 50% of organics by weight. Such a high fraction of organics would not allow producing of compact films of PbS(S) CQDs, which are necessary for the fabrication of electronic and optoelectronic devices. We have found that washing PbS(S) CQDs with much less polar ethyl acetate allows us to bring the inorganic content to about 80%, which is comparable to conventional Pb-rich PbS CQDs

(Figure S4). Despite the low quantity of free ligands, these purified CQDs are still soluble in nonpolar organic solvents, which are typically utilized for CQD thin-film deposition, such as hexane, chloroform, and toluene. In contrast, PbS(S) CQDs washed with ethanol were soluble only in chloroform and quickly agglomerated in hexane.

In addition to morphological changes, the sulfurization of oleate-capped PbS CQDs has a tremendous effect on optical properties. Oleate-capped PbS CQDs display a clear excitonic peak in the absorption spectrum and a single band in the emission spectrum (Figure 1F). In contrast, the peak corresponding to the first excitonic transition is absent in the absorption spectrum of S-rich PbS(S) CQDs, while photoluminescence could not be detected at all in our conditions. This is an indication of the variation of the density of states due to sulfurization, which results in the transformation of the semiconducting oleate-capped PbS CQDs into semimetallic nanocubes.^{8,21}

FETs were fabricated in order to test the transport properties of our novel S-rich PbS(S) CQDs. The output curves of the devices are shown in Figure 2A. It is important to

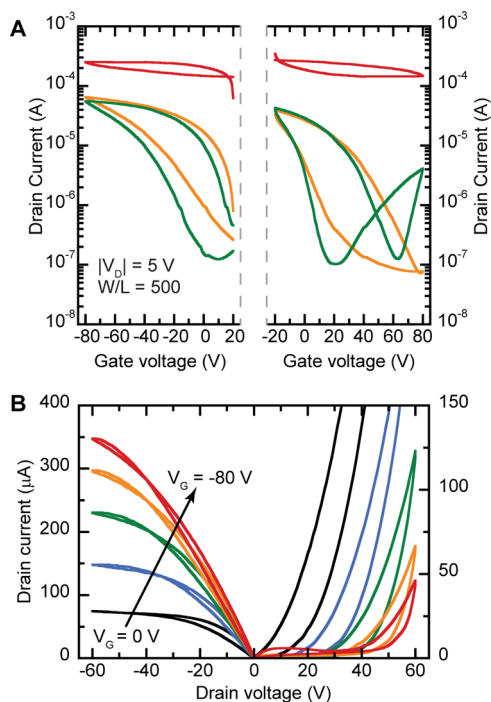


Figure 2. (A) Transfer characteristics of the pristine PbS CQD FETs prepared with native S-rich PbS(S) CQDs (red) and after the treatment with 50 mM PbI₂ solution and annealing at 120 °C for 1 min (orange) and 20 min (green). (B) Output characteristics of S-rich PbS(S) CQDs and after the treatment with 50 mM PbI₂ solution and annealing at 120 °C for 1 and 20 min.

point out that no extra treatment of the film was performed in this case. Therefore, the CQDs are expected to be capped with long insulating ligands. The surprisingly high source–drain current in this sample indicates a high charge carrier concentration in the active layer. This observation is in agreement with calculations showing that highly nonstoichiometric PbS CQDs should result in metallic transport. In this work, 230 nm of thermally grown SiO₂ was used as a gate dielectric, but highly doped films of PbS CQDs require a gate

dielectric with much higher gate capacitance to be able to modulate the current effectively.^{19,21,31}

An interesting question is whether the off-stoichiometry could be tuned down by chemical treatments. The surface of the S-rich PbS(S) CQDs should have a strong affinity to Lewis acids. We selected PbI₂ because we surmised that it would bind to the surface sulfur atoms via Pb as a Z-type ligand, and at the same time, iodide would passivate Pb atoms providing an overall good passivation of the CQD surface. Ligand exchange with PbI₂/DMF solution is accompanied with disappearance in the FTIR spectra of the peaks assigned to the C–H vibrations (Figure S5). The shape of nanocrystals does not change (Figure S6). Drying of the film at 120 °C for 1 min is not sufficient to remove solvent molecules from the film due to the relatively high boiling point of DMF (153 °C). Further device annealing for 20 min at the same temperature results in a lower off-state current and appearing of the electron current. The transfer characteristics of the device using S-rich PbS(S) CQDs treated with 50 mM PbI₂ solution are shown in Figure 2A. Overall the ambipolar transport has a dominance of positive charge carriers with low hysteresis for holes (Figure 2B).

In order to verify whether the enhancement in electron current is caused by PbI₂ complexes,³² iodide anions, or the solvent itself, we have performed several additional experiments. First, ligand exchange with other iodide ligands was performed: pristine films of S-rich PbS(S) CQDs were treated with 20 mM tetrabutylammonium iodide solution in methanol for 1 min. These films, however, do not show a difference in transport from the pristine PbS(S) films washed with pure methanol. This observation is in line with the decoration of the surface of the S-rich PbS(S) CQDs with sulfur and not with lead atoms.

The treatment of PbS(S) films with pure DMF resulted in cracking and delamination of the films. However, a part of the films was left between the interdigitated source/drain electrodes allowing electrical measurements. Importantly, washing with DMF did not change the charge carrier balance and did not result in the formation of a clear “off” state but only lowers the current. At the same time, it is important to note that such washing has two side effects. First, the CQD film washed with DMF visually looks “dissolved”, which may indicate that sulfide- or polysulfide-capped PbS(S) CQDs may be partially washed out by such a polar solvent although they did not form a stable colloidal solution in DMF. Second, potentially present polysulfide anions are likely washed away by DMF, which is evidenced by its blueish color. The blueish solution obtained by mixing PbS(S) CQDs with DMF was filtered through the 0.2 μm PTFE filter, and the absorption spectrum was taken. The absorption spectrum contains a peak at 615–620 nm, which disappears quickly upon exposure of the solution to air (the spectra before and after the air exposure as well as photographs of the vials are shown in Figure S7). The peak at around 617 nm is assigned to the trisulfide radical anion (S₃^{•-}) in basic organic polar solvents.^{33,34} Disappearance of this absorption peak after the air exposure is due to the rapid oxidation of trisulfide species.³⁵

As PbI₂ can recap PbS(S) CQDs and alter their electron transport, we have studied the effect of PbI₂ concentration on the carrier mobility in PbS(S) films (Figure 3A). At a low concentration of PbI₂, the hole mobility is much larger than the electron mobility. Notably, the treatment with low concentration of PbI₂ results in severe cracks and partial delamination of the film (Figure S8), similar to the effect

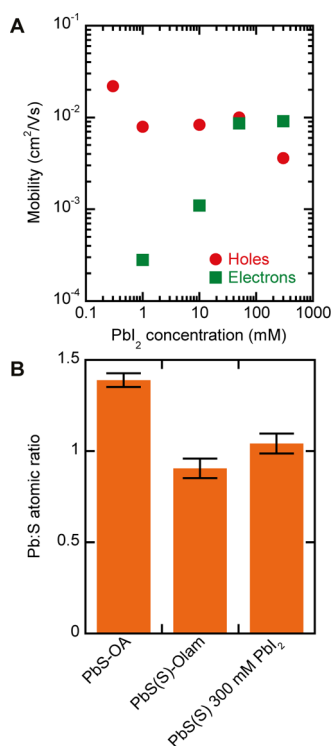


Figure 3. (A) Dependence of the linear mobility values on the concentration of PbI₂ ligand solution. (B) Quantification of Pb/S atomic ratios by Rutherford backscattering spectrometry (RBS).

observed in the case of washing with pure DMF. Upon increasing the PbI₂ concentration, the hole mobility stays around 1×10^{-2} cm²/Vs, while the electron mobility gradually increases. A qualitatively similar but opposite trend was observed during the treatment of Pb-rich PbS CQDs with HS⁻ ligands, where electron mobility stayed in the same range and the hole mobility was modulated.²¹ The value of the hole linear mobility in our samples is comparable to the one of the Na₂Se-treated PbSe CQD FETs¹⁸ and is an order of magnitude lower than the one of the record HS⁻ treated PbS devices, which employ ion gel gating with much higher capacitance.²¹ Using a highly concentrated 300 mM PbI₂ solution for the ligand exchange results in higher electron mobility than the hole mobility. Therefore, we can conclude that the treatment with PbI₂ changes the surface composition by introducing Pb atoms.

EDX analysis was performed to track the change of the stoichiometry after the sulfurization of PbS-OA and ligand exchange of S-rich CQDs (Figure S9). Noteworthy, the Pb to S ratios were obtained by using a standardless quantification when all the samples were measured in exactly the same conditions and processed in the same way (more details can be found in the Experimental Methods section). The sulfurization of PbS-OA results in a significant drop of the Pb to S ratio, which corresponds to the increased sulfur content in S-rich PbS(S) CQDs. Ligand exchange of these S-rich CQDs with 300 mM PbI₂ solution leads to a slight increase of the Pb to S ratio, indicating a minor rise in lead content in the sample and retention of the S-rich nature of the CQDs.

The atomic Pb to S ratios were further quantified by RBS, which is a more precise analytical technique for the elements involved here. Figure 3B summarizes the results from two separate sets of measurements. In the first set (Figure S9), 2.9

nm large oleate-capped PbS CQDs possess a Pb/S atomic ratio of 1.41, which is in a good agreement with the model values for these sizes of CQDs.²⁸ The sulfurization of this sample reduces the Pb/S atomic ratio in PbS(S)-Olam to 0.94. This sulfurization is accompanied with the ripening of CQDs to a cubic shape with an edge size 8.6 nm. We note that the Pb/S ratio is known to be size-dependent for conventional PbS CQDs capped with lead oleate. However, in that case, the Pb/S ratio always stays above 1 (Pb-rich composition), reaching 1.1–1.26 for ~8 nm large CQDs.^{28,29} Our method allows achieving S-rich stoichiometry while retaining the colloidal stability of CQDs. The second set of the samples for RBS was prepared later in order to check the effect of ligand exchange with PbI₂ ligands on the stoichiometry of CQDs. In this case (Figure S10), oleate-capped PbS CQDs and in PbS(S)-Olam possess atomic ratios of 1.37 and 0.87, respectively, showing the reproducibility of the experiment. After the solid-state ligand exchange with concentrated PbI₂ solution, the Pb/S atomic ratio went to 1.04 without significant change of the size and morphology of CQDs (Figure S6), which could be assigned to the formation of an incomplete extra Pb layer in agreement with the transport properties of FET using as active PbI₂-exchanged S-rich PbS(S) CQDs.

CONCLUSIONS

To conclude, we successfully developed the synthesis of novel S-rich PbS CQDs through the sulfurization of oleate-capped PbS CQDs. The sulfurization alters their shape from spherical to cubic with preservation of the PbS rock salt crystal structure. The size of CQDs remains unchanged for medium size particles (~5 nm), whereas smaller CQDs (~3 nm) rip and grow notably. We found that the first excitonic peak in absorption disappears and the photoluminescence is quenched in S-rich PbS(S) CQDs. These optical properties and compositional analysis indicate a change of the stoichiometry to the extent that CQDs reach semimetallic-like density of states. The electrical transport properties of these S-rich CQDs are hole-dominated and can be well controlled by the solid-state ligand exchange with PbI₂ ligands. The electron mobility can be tuned within almost two orders of magnitude, while the hole mobility remains roughly around 1×10^{-2} cm²/Vs. Most importantly, our ligand-exchange protocol only slightly increases the Pb content in the film and therefore does not reduce the degree of p-doping. This method can be used for the hole transporting layer of PbS CQD solar cells, p-type thermoelectrics, and other devices in which both n- and p-type doping is required.

ASSOCIATED CONTENT

Supporting Information

The Supporting Information is available free of charge at <https://pubs.acs.org/doi/10.1021/acs.chemmater.0c03865>.

Materials characterization (particle size distribution, additional TEM micrographs, electron diffraction, FTIR spectra, and EDX), optical images of the CQD films, and RBS spectra of the films (PDF)

AUTHOR INFORMATION

Corresponding Authors

Maksym V. Kovalenko – Department of Chemistry and Applied Biosciences, ETH Zürich, Zürich 8093, Switzerland; Empa-Swiss Federal Laboratories for Materials Science and

Technology, Dübendorf 8600, Switzerland; orcid.org/0000-0002-6396-8938; Email: mvkovalenko@ethz.ch

Maria A. Loi – Zernike Institute for Advanced Materials, University of Groningen, 9747AG Groningen, The Netherlands; orcid.org/0000-0002-7985-7431; Email: m.a.loi@rug.nl

Authors

Dmytro Bederak – Zernike Institute for Advanced Materials, University of Groningen, 9747AG Groningen, The Netherlands

Dmitry N. Dirin – Department of Chemistry and Applied Biosciences, ETH Zürich, Zürich 8093, Switzerland; Empa-Swiss Federal Laboratories for Materials Science and Technology, Dübendorf 8600, Switzerland; orcid.org/0000-0002-5187-4555

Nataliia Sukharevska – Zernike Institute for Advanced Materials, University of Groningen, 9747AG Groningen, The Netherlands

Jamo Momand – Zernike Institute for Advanced Materials, University of Groningen, 9747AG Groningen, The Netherlands

Complete contact information is available at:
<https://pubs.acs.org/10.1021/acs.chemmater.0c03865>

Author Contributions

[†]D. B. and D. N. D. contributed equally to this work.

Notes

The authors declare no competing financial interest.

ACKNOWLEDGMENTS

The authors are thankful to Arjen Kamp, Dr. Teodor Zaharia, and Gert ten Brink for the technical support. Prof. Bart J. Kooi is acknowledged for the access to TEM in his group. The Groningen team is grateful for the financial support of the Dieptestrategie program from Zernike Institute for Advanced Materials. We acknowledge Dr. Maryna Bodnarchuk for electron microscopy at the Empa Electron Microscopy Center and Dr. M. Döbeli for taking RBS spectra at Ion Beam Physics Center (ETHZ).

REFERENCES

- (1) Kovalenko, M. V.; Manna, L.; Cabot, A.; Hens, Z.; Talapin, D. V.; Kagan, C. R.; Klimov, V. I.; Rogach, A. L.; Reiss, P.; Milliron, D. J.; et al. Prospects of Nanoscience with Nanocrystals. *ACS Nano* **2015**, *9*, 1012–1057.
- (2) Liu, Z.; Yuan, J.; Hawks, S. A.; Shi, G.; Lee, S.; Ma, W. Photovoltaic Devices Based on Colloidal PbX Quantum Dots: Progress and Prospects. *Solar* **2017**, *1*, 1600021.
- (3) Sun, B.; Johnston, A.; Xu, C.; Wei, M.; Huang, Z.; Jiang, Z.; Zhou, H.; Gao, Y.; Dong, Y.; Ouellette, O.; et al. Monolayer Perovskite Bridges Enable Strong Quantum Dot Coupling for Efficient Solar Cells. *Joule* **2020**, *4*, 1542–1556.
- (4) Hines, M. A.; Scholes, G. D. Colloidal PbS Nanocrystals with Size-Tunable Near-Infrared Emission: Observation of Post-Synthesis Self-Narrowing of the Particle Size Distribution. *Adv. Mater.* **2003**, *15*, 1844–1849.
- (5) Cademartiri, L.; Montanari, E.; Calestani, G.; Migliori, A.; Guagliardi, A.; Ozin, G. A. Size-Dependent Extinction Coefficients of PbS Quantum Dots. *J. Am. Chem. Soc.* **2006**, *128*, 10337–10346.
- (6) Hendricks, M. P.; Campos, M. P.; Cleveland, G. T.; Jen-La Plante, I.; Owen, J. S. A Tunable Library of Substituted Thiourea Precursors to Metal Sulfide Nanocrystals. *Science* **2015**, *348*, 1226–1230.

(7) Bertolotti, F.; Dirin, D. N.; Ibáñez, M.; Krumeich, F.; Cervellino, A.; Frison, R.; Voznyy, O.; Sargent, E. H.; Kovalenko, M. V.; Guagliardi, A.; et al. Crystal Symmetry Breaking and Vacancies in Colloidal Lead Chalcogenide Quantum Dots. *Nat. Mater.* **2016**, *15*, 987–994.

(8) Kim, D.; Kim, D.-H.; Lee, J.-H.; Grossman, J. C. Impact of Stoichiometry on the Electronic Structure of PbS Quantum Dots. *Phys. Rev. Lett.* **2013**, *110*, 196802.

(9) Speirs, M. J.; Dirin, D. N.; Abdu-Aguye, M.; Balazs, D. M.; Kovalenko, M. V.; Loi, M. A.; Antonietta, M. Temperature Dependent Behaviour of Lead Sulfide Quantum Dot Solar Cells and Films. *Energy Environ. Sci.* **2016**, *9*, 2916–2924.

(10) Shulga, A. G.; Piveteau, L.; Bisri, S. Z.; Kovalenko, M. V.; Loi, M. A. Double Gate PbS Quantum Dot Field-Effect Transistors for Tuneable Electrical Characteristics. *Adv. Electron. Mater.* **2016**, *2*, 1500467.

(11) Balazs, D. M.; Nugraha, M. I.; Bisri, S. Z.; Sytnyk, M.; Heiss, W.; Loi, M. A. Reducing Charge Trapping in PbS Colloidal Quantum Dot Solids. *Appl. Phys. Lett.* **2014**, *104*, 112104.

(12) Chuang, C.-H. M.; Brown, P. R.; Bulović, V.; Bawendi, M. G. Improved Performance and Stability in Quantum Dot Solar Cells through Band Alignment Engineering. *Nat. Mater.* **2014**, *13*, 796–801.

(13) Liu, M.; Voznyy, O.; Sabatini, R.; García De Arquer, F. P.; Munir, R.; Balawi, A. H.; Lan, X.; Fan, F.; Walters, G.; Kirmani, A. R.; et al. Hybrid Organic-Inorganic Inks Flatten the Energy Landscape in Colloidal Quantum Dot Solids. *Nat. Mater.* **2017**, *16*, 258–263.

(14) Lu, K.; Wang, Y.; Liu, Z.; Han, L.; Shi, G.; Fang, H.; Chen, J.; Ye, X.; Chen, S.; Yang, F.; et al. High-Efficiency PbS Quantum-Dot Solar Cells with Greatly Simplified Fabrication Processing via “Solvent-Curing”. *Adv. Mater.* **2018**, *30*, 1707572.

(15) Aqoma, H.; Jang, S. Y. Solid-State-Ligand-Exchange Free Quantum Dot Ink-Based Solar Cells with an Efficiency of 10.9%. *Energy Environ. Sci.* **2018**, *11*, 1603–1609.

(16) Kirmani, A. R.; Sheikh, A. D.; Niazi, M. R.; Haque, M. A.; Liu, M.; de Arquer, F. P. G.; Xu, J.; Sun, B.; Voznyy, O.; Gasparini, N.; et al. Overcoming the Ambient Manufacturability-Scalability-Performance Bottleneck in Colloidal Quantum Dot Photovoltaics. *Adv. Mater.* **2018**, 1801661.

(17) Speirs, M. J.; Balazs, D. M.; Dirin, D. N.; Kovalenko, M. V.; Loi, M. A. Increased Efficiency in Pn-Junction PbS QD Solar Cells via NaHS Treatment of the p-Type Layer. *Appl. Phys. Lett.* **2017**, *110*, 103904.

(18) Oh, S. J.; Berry, N. E.; Choi, J. H.; Gauldin, E. A.; Lin, H.; Paik, T.; Diroll, B. T.; Muramoto, S.; Murray, C. B.; Kagan, C. R. Designing High-Performance PbS and PbSe Nanocrystal Electronic Devices through Stepwise, Post-Synthesis, Colloidal Atomic Layer Deposition. *Nano Lett.* **2014**, *14*, 1559–1566.

(19) Oh, S. J.; Berry, N. E.; Choi, J.-H.; Gauldin, E. A.; Paik, T.; Hong, S.-H.; Murray, C. B.; Kagan, C. R. Stoichiometric Control of Lead Chalcogenide Nanocrystal Solids to Enhance Their Electronic and Optoelectronic Device Performance. *ACS Nano* **2013**, *7*, 2413–2421.

(20) Stavrinadis, A.; So, D.; Konstantatos, G. Low-Temperature, Solution-Based Sulfurization and Necking of PbS CQD Films. *J. Phys. Chem. C* **2016**, *120*, 20315–20322.

(21) Balazs, D. M.; Bijlsma, K. I.; Fang, H.-H.; Dirin, D. N.; Döbeli, M.; Kovalenko, M. V.; Loi, M. A. Stoichiometric Control of the Density of States in PbS Colloidal Quantum Dot Solids. *Sci. Adv.* **2017**, *3*, No. eaao1558.

(22) Bederak, D.; Balazs, D. M.; Sukharevska, N. V.; Shulga, A. G.; Abdu-Aguye, M.; Dirin, D. N.; Kovalenko, M. V.; Loi, M. A. Comparing Halide Ligands in PbS Colloidal Quantum Dots for Field-Effect Transistors and Solar Cells. *ACS Appl. Nano Mater.* **2018**, *1*, 6882–6889.

(23) Doolittle, L. R. A Semiautomatic Algorithm for Rutherford Backscattering Analysis. *Nucl. Instruments Methods Phys. Res. Sect. B Beam Interact. with Mater. Atoms* **1986**, *15*, 227–231.

(24) Thomson, J. W.; Nagashima, K.; Macdonald, P. M.; Ozin, G. A. From Sulfur–Amine Solutions to Metal Sulfide Nanocrystals: Peering into the Oleylamine–Sulfur Black Box. *J. Am. Chem. Soc.* **2011**, *133*, 5036–5041.

(25) Si, H.-Y.; Yuan, D.; Chen, J.-S.; Chow, G.-M. Synthesis of PbS Nanocrystals from Sulfur–Amine Solutions at Room Temperature. *RSC Adv.* **2011**, *1*, 817.

(26) Kim, E. T.; Chung, W. J.; Lim, J.; Johe, P.; Glass, R. S.; Pyun, J.; Char, K. One-Pot Synthesis of PbS NP/Sulfur-Oleylamine Copolymer Nanocomposites via the Copolymerization of Elemental Sulfur with Oleylamine. *Polym. Chem.* **2014**, *5*, 3617.

(27) Yuan, B.; Tian, X.; Shaw, S.; Petersen, R. E.; Cademartiri, L. Sulfur in Oleylamine as a Powerful and Versatile Etchant for Oxide, Sulfide, and Metal Colloidal Nanoparticles. *Phys. Status Solidi Appl. Mater. Sci.* **2017**, *214*, 1600543.

(28) Beygi, H.; Sajjadi, S. A.; Babakhani, A.; Young, J. F.; van Veggel, F. C. J. M. Surface Chemistry of As-Synthesized and Air-Oxidized PbS Quantum Dots. *Appl. Surf. Sci.* **2018**, *457*, 1–10.

(29) Moreels, I.; Lambert, K.; Smeets, D.; De Muynck, D.; Nollet, T.; Martins, J. C.; Vanhaecke, F.; Vantomme, A.; Delerue, C.; Allan, G.; et al. Size-Dependent Optical Properties of Colloidal PbS Quantum Dots. *ACS Nano* **2009**, *3*, 3023–3030.

(30) Krieg, F.; Ochsenein, S. T.; Yakunin, S.; ten Brinck, S.; Aellen, P.; Süess, A.; Clerc, B.; Guggisberg, D.; Nazarenko, O.; Shynkarenko, Y.; et al. Colloidal CsPbX₃ (X = Cl, Br, I) Nanocrystals 2.0: Zwitterionic Capping Ligands for Improved Durability and Stability. *ACS Energy Lett.* **2018**, *3*, 641–646.

(31) Balazs, D. M.; Loi, M. A. Lead-Chalcogenide Colloidal-Quantum-Dot Solids: Novel Assembly Methods, Electronic Structure Control, and Application Prospects. *Adv. Mater.* **2018**, *30*, 1800082.

(32) Dirin, D. N.; Dreyfuss, S.; Bodnarchuk, M. I.; Nedelcu, G.; Papagiorgis, P.; Itskos, G.; Kovalenko, M. V. Lead Halide Perovskites and Other Metal Halide Complexes As Inorganic Capping Ligands for Colloidal Nanocrystals. *J. Am. Chem. Soc.* **2014**, *136*, 6550–6553.

(33) Chivers, T.; Drummond, I. The Chemistry of Homonuclear Sulphur Species. *Chem. Soc. Rev.* **1973**, *2*, 233.

(34) Chivers, T.; Drummond, I. Characterization of the Trisulfur Radical Anion S₃⁻ in Blue Solutions of Alkali Polysulfides in Hexamethylphosphoramide. *Inorg. Chem.* **1972**, *11*, 2525–2527.

(35) Gaillard, F.; Levillain, E.; Lelieur, J. P. Polysulfides in Dimethylformamide: Only the Radical Anions S₃⁻ and S₄⁻ Are Reducible. *J. Electroanal. Chem.* **1997**, *432*, 129–138.